

MULTIVARIABLE DEPENDENCE AND CONTRIBUTING FACTORS OF BILAYER
GRAPHENE FRICTIONAL BEHAVIOR

Connor Fitzpatrick Toro Miller

A THESIS

Presented to the Faculty of Miami University in partial
fulfillment of the requirements
for the degree of

Master of Science

Department of Mechanical and Manufacturing Engineering

The Graduate School
Miami University
Oxford, Ohio

2024

Dr. Zhijiang Ye, Advisor
Dr. Mark Sidebottom, Reader
Dr. Andrew Paluch, Reader
Dr. Timothy Cameron, Reader

©

Connor Fitzpatrick Toro Miller

2024

ABSTRACT

The friction and wear properties of bilayer graphene on silicon substrate with diamond atomic force microscope tip were investigated using molecular dynamic simulation with three independent variables of tip velocity, temperature, and normal load. Based on isolated experimental results, it is determined that graphene friction is velocity, temperature, and normal load dependent. Velocity and normal load increase lead to positive friction correlations while temperature increase leads to negative friction correlations, thus leaving the mechanism to be determined. Combined studies reveal similar results, with each variable maintaining its isolated effect in chorus with the other utilized. Upon obtaining the contact area from these experiments it is evident that velocity and temperature change do not hold direct bearing on the contact area, rather that it is the normal load and size of the sliding surfaces that can fluctuate both contact area and friction in tandem. Hence, the mechanism with respect to velocity and temperature dependence of graphene friction is determined to be variation in interatomic potentials associated with interatomic interactions. Varying the contact area can increase or decrease the quantity of atoms in contact, therefore also having an impact on graphene friction.

Table of Contents

1 – Introduction.....	1
1.1 – Graphene Overview.....	1
1.2 – Molecular Dynamic Simulation	2
1.3 – Atomic Force Microscopy.....	3
1.4 – Graphene Frictional Behavior	4
1.5 – Contact Mechanics	7
1.6 – Problem Statement	9
2 – Methods.....	9
2.1 – Physical Experimentation.....	9
2.2 – Simulation Design	9
2.3 – Contact Area Calculation	14
3 – Results.....	15
3.1 – Velocity Dependent Friction	15
3.2 – Temperature Dependent Friction	17
3.3 – Normal Load Dependent Friction	20
3.4 – Combined Variable Dependence.....	23
3.5 – Contact Area Dependence	27
4 – Conclusions.....	33
5 – References.....	34

List of Tables

Table 1 – <i>Property list for graphene</i>	1
Table 2 – <i>Summary of independent variable fluctuations for data collection in LAMMPS</i>	13

List of Figures

Figure 1 – <i>General schematic showing the operating mode of an atomic force microscope</i>	4
Figure 2 – <i>MD simulation containing the AFM tip sliding over bilayer graphene on silicon substrate visualized in Ovito</i>	10
Figure 3 – <i>Dimensional visualization of AFM tip experiment in Ovito</i>	10
Figure 4 – <i>Free body force diagram of the AFM tip used in AFM simulation</i>	12
Figure 5 – <i>Friction curve depicting absolute force peaks and valleys seen with static and kinetic friction, as well as the saw-tooth pattern which is characteristic of stick-slip friction</i>	14
Figure 6 – <i>Scatter plot showing the contact atoms for a given timestep of a Lammmps dump file, the difference between the two outermost atoms is the contact diameter</i>	15
Figure 7 – <i>Friction force and friction coefficient varying at increasing velocity with constant temperature of 300 K and normal load of 177 nN</i>	17
Figure 8 – <i>Friction force and friction coefficient at increasing temperature with constant applied tip velocity of 1 m/s and normal load of 177 nN</i>	19
Figure 9 – <i>Friction force at increasing temperature with constant applied tip velocity of 50 m/s for a normal load of 885 nN</i>	20
Figure 10 – <i>Ovito visualization of graphene wear seen at 500 K and 885 nN</i>	20
Figure 11 – <i>Normal force dependence of graphene friction force and friction coefficient at constant temperature of 300 K and constant applied tip velocity of 50 m/s</i>	22
Figure 12 – <i>Ovito renderings for applied loadings of ~958 nN (a) and ~1013 nN (b)</i> ...	23
Figure 13 – <i>Friction force measured at varying temperatures and tip velocities with a constant normal load of 18.42 nN</i>	25
Figure 14 – <i>Friction force at varying tip velocities and temperatures for a velocity range of 1 to 50 m/s, normal load is set to 18.42 nN</i>	26
Figure 15 – <i>Friction force at varying temperature and applied normal load with constant applied tip velocity of 50 m/s</i>	26

Figure 16 – Mean friction compared to the contact area at a) 300 Kelvin, b) 400 Kelvin, and c) 500 Kelvin, figure 16 d) is a comparison of the contact area across all temperatures and normal loads prior to wear31

Figure 17 – – Wear points at each temperature and normal load with red x marks denoting wear points.....32

Figure 18 – Mean friction compared to the contact area at a) 300 Kelvin, b) 400 Kelvin, and c) 500 Kelvin, figure 18 d) is a comparison of the contact area across all temperatures and tip velocities, all tests were done at a normal load of 177 nN..... 32

Dedication

“What you think, you become. What you feel, you attract. What you imagine, you create.”

This thesis is dedicated to my mom and dad who never stopped believing in me regardless of how lofty my dreams were.

To all of those who I have constantly found myself surrounded by that never relented in pushing me to be the best version of myself, thank you.

Acknowledgements

I would like to first thank Dr. Ye for advising me and guiding me through this difficult process. Without his honesty, patience, and genuine care for my work, I would not have had the tools necessary to write this document.

Thank you to my committee members Dr. Sidebottom, Dr. Paluch, and Dr. Cameron for the help and opportunity they provided me with during this research.

I would also like to thank a few other people who helped guide me during this work. My peer Ashutosh Pitkar, thank you for mentoring me since my early days at Miami and answering all my odd questions. The Mechanical Engineering graduate program director, Dr. Zanjani, thank you for providing me with the opportunity to complete my graduate research at Miami University.

1 – Introduction and Background

1.1 – Graphene Overview

Graphene, or single atom thick layers of sp^2 -hybridized carbon atoms arranged in a hexagonal lattice, has been shown to have a variety of advantageous properties. These include high thermal conductivity as well as advantageous mechanical and electrical applications [1]. Graphene's prospect as a lubricant is also something that has been studied, and its friction as well as wear properties have been tested in various environments [2]. Graphene, along with many other 2-dimensional materials, has been the subject of research since 2004 [1], and now has thousands of related publications with countless application areas.

Shown in **Table 1**, graphene has excellent bulk material properties, including a Young's modulus roughly ten times as large as steel, tensile strength 100 times that of tungsten, and around 1000 times that of steel. Graphene also presents with a remarkably low density, making it an extremely light weight material, lighter than aluminum which is around 2.7 g/cm^3 [3]. This set of properties makes graphene ideal for use as a lubricant or coating, an application in which it is exposed to high stresses, extreme temperatures, and often great variation in surface velocity.

Property	Value	Unit
Young's Modulus	1	<i>TPa</i>
Tensile Strength	130	<i>GPa</i>
Density	~1.6 – 2.1	<i>g/cm³</i>
Surface Area	2,629	<i>m²/g</i>
Thermal Conductivity	~5,000	<i>W/mK</i>

Table 1 – *Property list for graphene* [4].

1.2 – Molecular Dynamic Simulation

Molecular dynamic simulation or MD simulation is a method of computer simulation in which the movements of atoms and molecules are analyzed. MD simulation uses simple kinematics to break down a complex system of atoms into point masses, allowing for their behavior over time to be easily modeled. The behavior of the atoms in the simulation can be used to understand certain quantitative and qualitative characteristics of the system at hand such as internal energy, intermolecular forces, crystalline structure, and much more. MD simulations are often complex in nature and require high levels of computing power to execute simulations in a timely fashion, making it essential to use some kind of high-level computing cluster.

MD simulation programs use different potential models to dictate intermolecular interactions. This study utilizes a few different potential models to dictate system behavior. Among these are Lennard-Jones potential model, and adaptive intermolecular reactive bond order (AIREBO) potential. The Lennard-Jones potential model expresses that atoms generally experience weak van der Waals attraction and have either positive potential or no potential energy from the atomic radius to infinity, and strong repulsion with negative potential energy at distances less than the atomic radius due to the overlapping of electron clouds [5]. The main importance of LJ potential is that it is a great model of pairwise intermolecular potentials at distances greater than a given atomic radius but begins to behave erratically upon two atoms entering each other's radii. This brings about the need for different variations of LJ potential models. Among these are LJ potential with a set cutoff point, or "LJ/Cut", and LJ potential models suitable with long range corrections typically used for modeling simulations with water [5],[6]. The AIREBO potential model differs from the LJ potential model primarily because it is a many-bodied potential used to model interactions between many different atoms both bonded and un-bonded in a system, making it capable of modeling both intermolecular and intramolecular interactions in a system [7],[8]. AIREBO excels primarily at modeling covalently bonded atomic systems in the context of MD simulation and is hence utilized to covalently bond the required groups in the input simulation file. AIREBO potential is thus primarily utilized for the study of hydrocarbons and related hydrocarbon-based systems, of which is the primary element of focus in this study.

The MD simulation used for this study uses all three of these potentials in tandem with one another to model interactions between different parts of the system. These specific use cases and

interactions will be discussed in the methods section of this thesis. The use of MD simulation in this context allows for a multitude of tests to be run simultaneously on a large computing cluster. This gives the ability to test experimental parameters for later use in physical experimentation, and rapidly establish several data points to understand system behavior. MD simulation also opens the door for the boundaries of testing to be pushed, with parameters such as velocity and temperature that may exceed what is possible in real world testing with given cost and time constraints.

1.3 – Atomic Force Microscopy

Atomic force microscopy (AFM) is a high-resolution version of scanning probe microscopy that can produce both morphology and force curves of a given nanoscale material surface, both of which essentially provide the user a topographical map of the measured interface. An AFM is used in this study as a basis for tests done using molecular dynamic simulation as well as physical experiments done to confirm findings from MD simulation in further work.

AFM and scanning probe microscopy have a few different modes of operation, all of which can be used to provide different data points relating to the surface properties of a given sample. The AFM has two modes of contact: tapping mode, and non-contact mode. In tapping mode, the cantilever is vibrated at or near resonance, causing it to meet the surface periodically [10]. The main goal of tapping mode is to negate any friction forces that would arise while scanning a sample, hence it was not used study. The main mode of importance in this study is contact mode in which the tip of the AFM is dragged over the surface of the sample. As the tip traverses the sample face, it moves up and down, flexing the attached cantilever beam much like the suspension on a car goes over bumps in the road. A laser reflects off the end of the cantilever nearest to the tip onto a photodetector. Contact mode can produce both morphological and friction force curves of the material surface, making it the ideal mode for use in this study. **Figure 1** shows contact mode and the forces exerted during operation.

The main force being measured as a part of this study will be the lateral force of friction presented in the x axis, that is the force that opposes the path of travel of the AFM. This friction force at the nanoscale is heavily dependent on the atomic level topography of the material over which the tip is dragged, including properties like the internal energy and lattice structure of the

system, and experimental parameters such as AFM tip velocity, and the normal force between the tip and the sample as well as the surrounding environmental temperature.

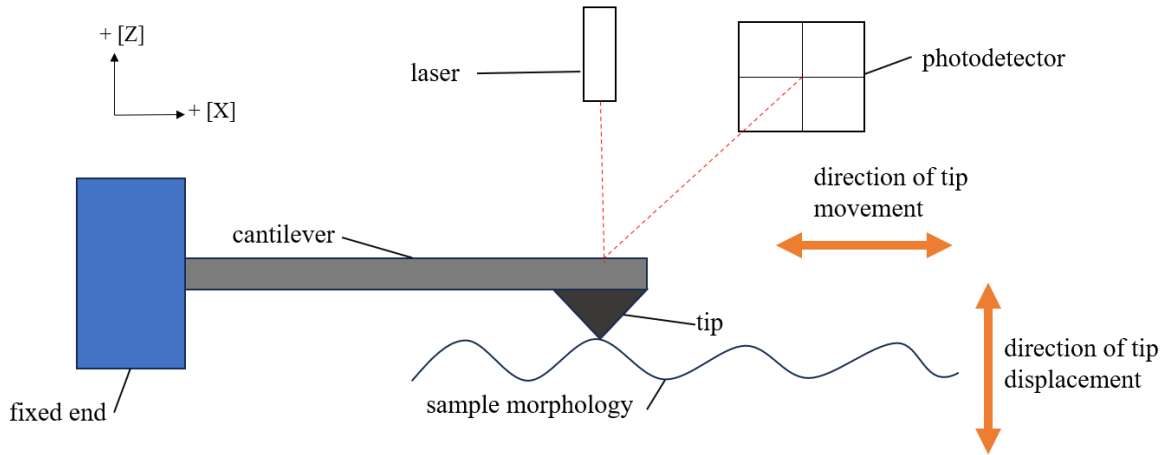


Figure 1 – *General schematic showing the operating mode of an atomic force microscope.*

1.4 – Graphene Frictional Behavior

Graphene and its frictional behavior under applied loads, varying AFM tip speed, and temperature are of great interest because of the material properties mentioned in **Table 1**. Graphene has a high Young’s modulus, thermal conductivity, and surface area, leading to an interest in its use in repeated wear applications as a potential coating or lubricant [11]. Thus, the question is raised of how graphene behaves when independent variables such as temperature, applied force, and tip velocity, are varied in both isolated and combined fashion, like the conditions that it would be exposed to as a lubricant in a real-world application.

Because graphene is a two-dimensional material, it is utilized in layers. Each layer is one atom thick, and the properties exhibited by a graphene sheet are largely dependent on the number of layers present. In previous studies, it has been shown that as the number of layers of graphene increases, the friction decreases in most cases [11], [12]. This has been confirmed by both molecular dynamic simulation and physical experimentation with an AFM. The underlying substrate roughness is also a big factor in the friction exhibited by a graphene sample as it is extremely difficult to isolate a graphene sheet and conduct an AFM scan on it without some kind

of underlying substrate. Ye et al. determined that a substrate with a large roughness relative to the others tested (.4 nm) was found to experience a decrease in friction by a factor of two when increasing the number of graphene layers from one to three [12]. Conversely, a substrate with a roughness as low as .1 nm or even an atomically smooth substrate experiences an increase in friction by a factor of ~1.5 when increasing the number of layers from one to three. This concludes that when graphene lays over top of a rough substrate, it almost acts as a blanket, filling in any roughness present, causing a net decrease in frictional force exerted by the sample. Almeida et al. confirms this correlation, with AFM experiments testing graphene layer counts to four under the same substrate roughness and finding that there is a negative linear correlation between friction force and layer count [11]. A higher roughness substrate will need two to four layers of graphene to see a decrease in friction, while a low roughness substrate or one that is atomically smooth would be better off with no graphene or a layer count below two. In the case of the simulations done in this paper, layer counts are always set to two.

The velocity of the surfaces being observed is another key factor when considering friction. Friction force tends to increase with velocity in the case of graphene samples in AFM experiments [11]. This correlation also adheres to the previously discussed relationship between layer count and friction, with a given velocity seeing a decrease in friction with increasing layers. Topological defects such as Stone-Wales defects, single vacancy defects, multi-vacancy defects, and line defects [13]. Stone-Wales defects occur because of the rotation of a single pair of carbon atoms in the lattice, rendering adjacent pairs of pentagonal and heptagonal carbon rings [14]. Single and multi-vacancy defects can both result in the formation of shapes that differ from the usual hexagonal lattice structure [14]. Line defects come about when graphene begins to form in different orientations during chemical vapor decomposition, which is a form of graphene synthesis. These differing orientations can stack on top of each other, eventually forming a line as different crystallographic orientations form in different locations and chain together [14]. Finally, out of plane carbon atoms can cause atoms to stack on top of the existing one atom thick sheet, resulting in a graphene sheet thickness greater than one atom [14]. All these defects can cause graphene sheets to behave in a way that differs from what is otherwise considered typical. It is important to know that for both previously discussed relationships, the assumption is made that there are no defects in the graphene sheets utilized. Although outside of the scope of this paper, graphene can

present with many defects, most of which increase the friction when they are present in AFM experimentation, causing the sample to differ from expected behavior.

This brings up the question of how graphene will behave with fluctuations in temperature as temperature tends to go up with velocity when two surfaces are sliding past each other. When any given solid atomic lattice experiences an increase in thermal energy, the atoms vibrate at a higher rate, causing a lower yield strength, higher incidence of atomic defects, and a system that overall does not behave as it would under room temperature conditions or 300 Kelvin. Graphene is no exception to this, which raises the question of how temperature impacts the frictional behavior of graphene. This relationship is not quite as cut and dry as those discussed previously, with some studies concluding varying results, and others drawing some kind of correlation whether it be positive or negative [15]. One study draws the conclusion that at varying normal force levels, unsupported graphene experiences an increase in friction force due to a thermally induced dynamic rippling, resulting in the tip to not only interact with the graphene sheet below, but also the thermally excited ripples in front [16]. This thermally induced dynamic rippling diminishes in supported graphene but is still present to a certain degree. This causes the friction force to decrease because of ripples not being as prevalent, causing the correlations to be opposite for supported and unsupported graphene. Regardless of what the relationship is, increasing the energy of a graphene sample can potentially result in atoms entering a more excited state, leading to thermally induced dynamic rippling, causing them to obstruct the movement of the AFM tip, increasing the existing friction force [17].

Increasing the normal force between two sliding surfaces, as expected, increases the friction between these two surfaces as the normal force and friction force are correlated to each other. This relationship does not quite behave as expected however, as a material like silicon has a much higher slope on a normal force vs friction curve than graphene does, indicating that graphene is somewhat unique [18]. Other studies show that graphene's frictional characteristics in this context are heavily dependent on substrate [16]. Particularly, graphene experiences increasing friction under elastic, rigid, and no substrate, with each group experiencing a transition from a low, linearly increasing friction force regime, to a high friction force regime nearly three times higher. This indicates strongly that friction force in the context of increasing normal force depends heavily on substrate and does not behave in linear fashion across all possible applied normal force values.

Exerting a force on a given area of graphene that results in a pressure exceeding the yield strength of 1.3 TPa can cause the graphene to wear or yield under the force of the tip [19]. This yielding can cause the now compromised graphene layers to buckle as the tip continues to move laterally across the sheet. The point at which this wear occurs may vary with temperature, tip velocity, and normal force.

1.5 – Contact Mechanics

Contact mechanics in a general sense govern the deformation of two contacting bodies. It is a widely studied and publicized field with many different theories governing a variety of contact scenarios. Hertzian contact mechanics deal with forces applied between curved surfaces where the contact area is significantly smaller than the object applying force. This results in exceptionally large stress concentrations, leading to a need for governing equations differing from typical stress calculations [20]. When conducting AFM experimentation, specifically in the instance of utilizing MD simulation, Hertzian contact mechanics must be brought into play as it is safe to assume that the contact area is infinitesimal, causing a potentially massive stress to be exerted on the sample.

The governing equation for Hertzian contact radius dictates that the applied force and radius are related by (equation 1) [20],[21].

$$r_{contact} = \left(\frac{3F}{8} * \frac{\frac{1 - \nu_1^2}{E_1} + \frac{1 - \nu_2^2}{E_2}}{\frac{1}{d_1} + \frac{1}{d_2}} \right)^{\frac{1}{3}} \quad (1)$$

Where F is the force applied, ν is Poisson's ratio, E is the Young's modulus, and d is the radius of surface. In the case of the AFM, the radius of the graphene face is assumed to be infinite because it is a flat surface. This leads to the second equation, which dictates the maximum stress of a given surface as a function of the radius and applied force (equation 2) [21].

$$p_{max} = \frac{3F}{2\pi r_{contact}^2} \quad (2)$$

This equation allows for the maximum stress concentration at a given force to be determined. The main goal of using these equations is to understand what normal force

might cause graphene wear by comparing the value for this maximum stress concentration to the value cited as the yield stress of graphene in **Table 1**.

Two things that Hertz contact theory fails to consider are surface adhesion energy, and large normal loads. The JKR, or Johnson-Kendall-Roberts model, factors in short range adhesive contact behavior, while the DMT, or Derjaguin, Muller and Toporov model, governs long range adhesive interactions. These models are governed by equations 3 and 4 respectively.

$$r_{contact}^3 = \frac{3R_{ef}}{4E} \left[F_n^{JKR} + 6\gamma\pi R_{ef} + \sqrt{F_n^{JKR} 12\gamma\pi R_{eff} + (6\gamma\pi R_{eff})^2} \right] \quad (3)$$

$$r_{contact}^3 = \frac{3R}{4E} (F + 4\gamma\pi R) \quad (4)$$

Where R_{ef} and R denote the effective radius and contact distance respectively, E denotes Young's modulus, and F_n^{JKR} and F denote the normal component of JKR force and normal load respectively. γ is also used to denote the adhesion energy between the two surfaces. Equations 3 and 4, while they are derived from the Hertz contact radius equation, do factor in adhesion in the form of the adhesion energy term. This allows for short- and long-range interactions, as well as increased normal load interactions to be accurately modeled. Idealistically, a combination of these two sufficiently reproduce the LJ potential curve, effectively governing most non-covalent interactions in a given atomic system.

There remains a question as to if a given sample temperature, or velocity can also influence the contact radius. Increases in temperature result in a net reduction of mechanical strength properties and an increase in plastic properties of a material [22]. This indicates that there may be an increase in the Hertzian contact radius with increasing temperature since Hertz contact radius and Young's modulus are inversely related (equation 1). The end goal of observing the Hertzian contact radius in this case is to understand if it has a relationship with the friction exerted at a given velocity. If this is the case, then Hertzian contact radius fluctuations can provide a strong indication as to graphene's friction and wear behavior.

1.6 – Problem Statement

The central idea of this research is to conduct a comprehensive factorially designed experiment that tests the friction behavior of graphene in relation to fluctuating independent variables. The independent variables of temperature, AFM tip velocity, and normal load will be used to determine if there is a root cause for friction increase such as a fluctuating contact area between graphene interface and silicon tip or if the fluctuating friction can be attributed to changes in interatomic potential. The findings from this study serve to discern what graphene's limiting factors are with regards to its broader application as a coating or lubricant, and if one or more of these external variables can be utilized to control this.

2 – Methods

2.1 – Physical Experimentation

Atomic force microscopy, as it has been previously discussed in section 1.2, is used twofold in this research. Primarily, the AFM is used as a model for the MD simulation configuration utilized. The real-world AFM will be used on the other hand to conduct verification experiments for the MD simulations conducted. The development of graphene samples in this context is rudimentary and is focused mainly on loosely replicating the results from the MD simulation work done thus far. Further work will likely delve further into physical experimentation as a tool and maybe even a source of data collection and simulation validation, but for now, it remains a guideline for simulation parameters.

2.2 – Simulation Design

All MD simulations discussed this research were done using Lammmps and visualized in Ovito or VMD. Within the MD simulation, the AFM is simplified down to a bilayer graphene configuration sitting on top of a silicon substrate with the silicon AFM tip dragging across the top

surface. The simulation runs much like the actual AFM, with the tip going back and forth at varying velocities. This format allows for the AFM tip to be dragged over the graphene surface several times in one simulation run, allowing for the testing of different velocities and normal forces. This study involves three independent variables, rendering it necessary to use factorial experimental design [23]. Factorial experiments contain more than one independent variable and observe the interaction between these independent variables as well as the impact on the dependent variables involved in the study.

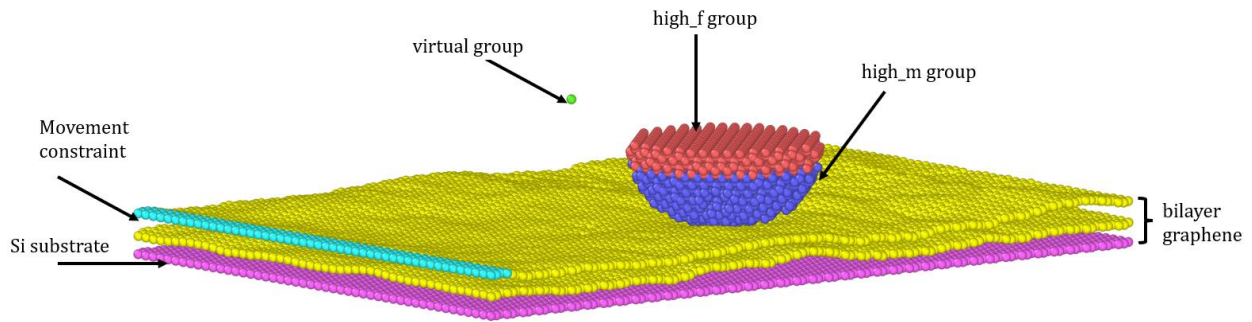


Figure 2 – MD simulation containing the AFM tip sliding over bilayer graphene on silicon substrate visualized in Ovito.

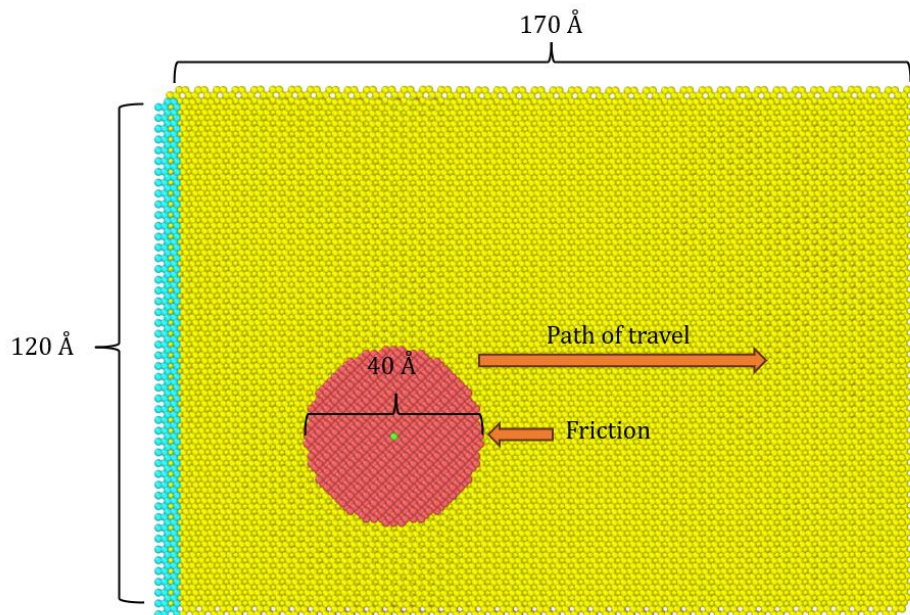


Figure 3 – Dimensional visualization of AFM tip experiment in Ovito.

The simulation used to obtain the data discussed in this study is conducted in a 120 Å (12 nm) by 170 Å (17 nm) box. This simulation box is comprised of a bilayer graphene configuration that sits on top of a silicon substrate. Friction, as previously mentioned, is measured via the AFM tip, which is 40 Å (4 nm) in diameter in this simulation. All these dimensional conditions are shown in **Figure 3**. Especially at the upper velocity ranges utilized, periodic boundary conditions must be considered, as the tip traveling outside of the simulation bounds can cause the simulation to be entirely unusable.

One of the governing principles of LAMMPS is the concept of atom types. Within each input file, a given atom will be created and assigned a type, this can be any real whole number, such as “type 1” for example. From here, atom types are grouped together into variable names. For the input file used in this simulation, these groups are virtual, high_f, and high_m seen in **Figure 2**. The high_f and high_m groups, also known as the high force and high mass groups, make up the two components of the tip, namely the component that contacts the graphene surface, high mass, and the group that downward forces are applied to, high force. Velocity fixes in the simulation are applied not to the tip itself, but to the virtual group, which is connected to the high force, and high mass, groups in the simulation file by way of a spring with a set stiffness constant. The reason for this is that all friction forces exerted by the graphene interface are translated from the tip to the virtual group, where the output variable is tied to, via the spring coupling, which exerts an equal and opposite force. For temperature variations in the simulation, a constant temperature in Kelvin is applied to the high mass and bilayer graphene groups as these are the two surfaces that interact during the simulation.

As previously discussed in the introduction, the MD simulation utilizes a few different potential models to dictate inter and intramolecular interactions, namely being LJ potential and AIREBO potential. Looking at **Figure 2**, the different groups are shown, with the tip being made up the high force, and high mass groups. The diamond tip is coupled or held together by the AIREBO potential model due to its previously discussed effectiveness at modeling covalent bonds [8]. The bilayer graphene atoms and silicon substrate atoms are also coupled using AIREBO potentials for the same reasons. Interactions between the tip and graphene interface as well as the graphene interface and underlying silicon substrate are governed by the LJ potential model because of its pertinence in dealing with atomic collisions and cutoff radii [5]. In this case, a cutoff radius

is set for these pairwise interactions between atoms across groups, allowing for accurate models of friction and wear to be produced.

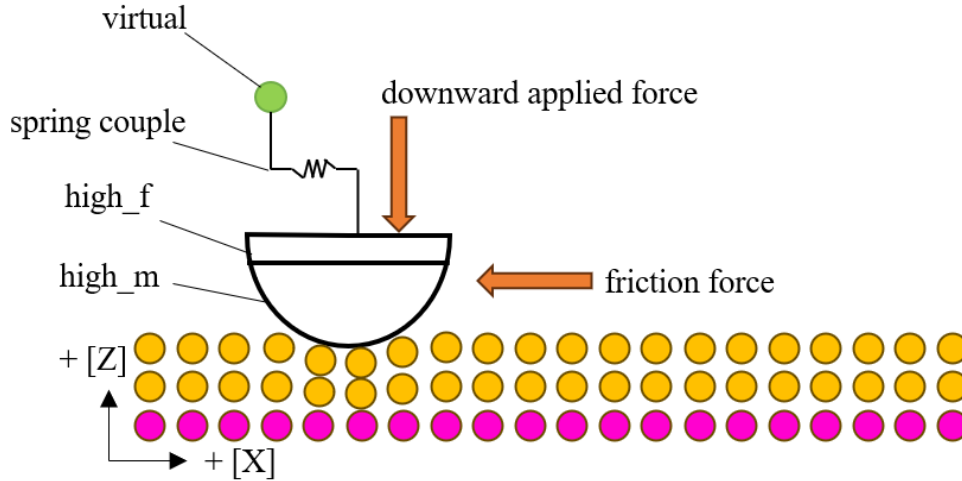


Figure 4 – Free body force diagram of the AFM tip used in AFM simulation.

Temperature, velocity, and normal force ranges were selected based on a few different factors. Temperature was selected to vary between 300 Kelvin and 500 Kelvin in increments of 50 degrees. Doing so allows for an understanding of graphene behavior under a range from room temperature all the way up to extremes found in harsh operating conditions. Velocity was also varied on a wide range for this study, with values ranging from .01 Angstroms per picosecond (1 m/s) to 1.6 Angstroms per picosecond (160 m/s). This velocity variation is rather large and is intended on replicating real world conditions that would not at all be attainable on a normal AFM. The normal force varies in the simulation from .05 eV/A to 1.0 eV/A which is .08 nN to 1.6 nN per atom in the high force group, making the actual force variation range from ~92.1 nN to ~1842.5 nN given that the force on each atom needs to be multiplied by the total number of atoms in the group. With how small the contact area is between the sample and AFM tip, the high range of 1842.5 nN far exceeds the elastic modulus of graphene (1.0 TPa). Each study done on MD simulation-based graphene friction and wear involves slightly different parameters from normal force to tip radii. The radius of the AFM tip directly indicates how much applied force will be needed to generate graphene wear due to the previously discussed inverse relationship between

pressure and area. Contact area is also going to fluctuate in this context, meaning that there may be a relationship between contact area and normal load. The full configuration of changing independent variables is summarized in **Table 2**. Another important parameter to discuss is the Gaussian velocity distribution of the atoms in the graphene sheet groups. This parameter is represented by a five-digit number in the input code which is used to create a Gaussian distribution of particle velocities. This, like the other parameters discussed above, must be changed for a different simulation result. If two simulations are submitted with exactly matching input codes including Gaussian distribution numbers, they will provide the exact same result every time they are run. Likewise, if two input codes are submitted with all parameters being the same, except their respective Gaussian distributions, they will provide different results.

Variable	Range	Unit
Velocity	2-120	<i>m/s</i>
Temperature	300-500	<i>K</i>
Normal Force	~10-1200	<i>nN</i>

Table 2-*Summary of independent variable fluctuations for data collection in Lammmps.*

When conducting a friction test in MD simulation, varying force curves are produced, creating the need to find some kind of steady state friction value for the entire simulation run. As previously specified, simulation runs involved in this study often tested 3 different velocity values in one simulation run, providing each an ample amount of time steps to reach a steady state. Within each of these runs, force curves are generated depicting an initial spike as initial static friction is broken and the tip oscillates, dissipating kinetic energy in the process. An example of the force curve for a given data set is shown in **Figure 5**. For the values presented in the figure, an average of the entire region is taken, including both the initial response and the steady state.

In addition to the peaks and troughs seen in **Figure 5**, there is also a jagged, saw-tooth fluctuation of friction. This fluctuation occurs due to stick-slip friction, a phenomenon that has been observed to occur in a variety of materials when using atomic force microscopy [24]. Stick slip friction can occur where kinetic friction is lower than static friction, with a heavy dependence on scanning speed [25]. In the results from this study, stick slip provides great fluctuation in

friction force measurements, which is why average friction is calculated over the absolute values of the whole data set.

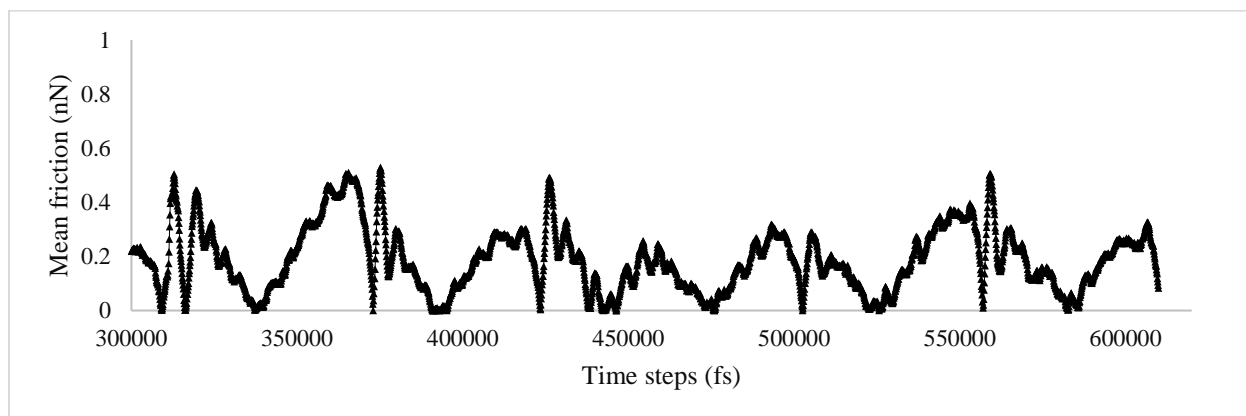


Figure 5 – Friction force curve depicting a generalized saw-tooth pattern that is characteristic of stick-slip friction governed by fluctuating exposure to inter-atomic potentials.

2.3 – Contact Area Calculation

The tertiary component of this study is calculating the contact area of various simulation outputs to understand if there is a relationship between contact area and mean friction force. As such, a MATLAB code was developed to calculate this value, as each dump file is thousands of lines long. The developed code takes the dump file and parses the atoms in the simulation off by type as discussed in the simulation design section. The user specifies which atom types are synonymous with the graphene sheet and tip groups. In this case, the tip type is 2, and the graphene interface is type 3. The code then uses loops to go through the entire dump file and determine on a consistent basis when atoms from each group are in contact. The positions of these atoms are stored, and the difference in positions between the two outermost atoms are stored as a variable for each time step to obtain an array with contact radius between the tip and the interface for the entire simulation as shown in **Figure 6**. An average of this array is calculated at the end, giving an average contact area for the entire simulation. In post data processing, this radius is used to calculate the average contact area for each simulation run.

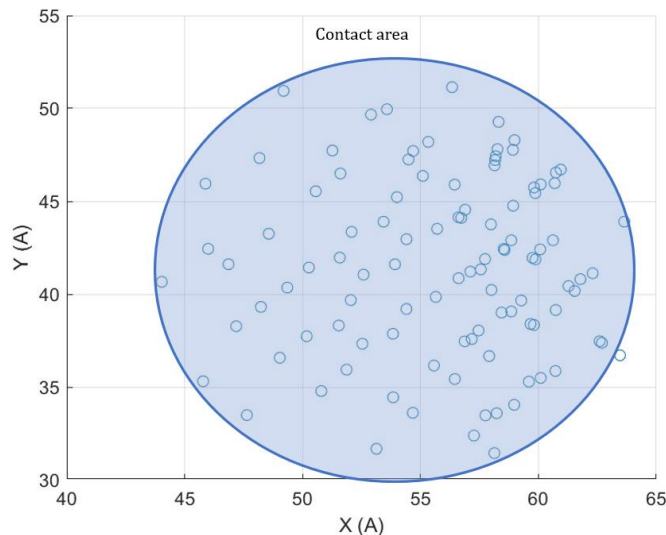


Figure 6 – Scatter plot showing the contact atoms for a given timestep of a LAMMPS dump file, the difference between the two outermost atoms is the contact diameter.

3 – Results

3.1 – Velocity Dependent Friction

In the world of tribology, especially when considering friction and wear mechanics, velocity is of utmost importance. Velocity often dictates key factors that govern lubricant performance such as wear rate and friction-based heat generation. Increasing and decreasing velocity often has ramifications on the performance of a lubricant, and moving from one significant velocity regime to another may result in an entirely different lubricant needing to be used. Velocity dependence becomes important when studying graphene’s friction performance as it is a key determinant of how it might behave in the context of lubrication.

The initial simulation-set tests graphene’s friction levels at varying AFM tip velocities, providing a clear understanding as to performance on both a low-end tip velocity, and the upper extremes of what may be seen in high velocity lubricant applications. In prior work, velocity has been shown to have a positive correlation with friction on a logarithmic basis [11],[26]. Results from this research shown in **Figure 7** show a clear positive correlation between friction coefficient and tip velocity, with constant normal force and temperature of 300 Kelvin, which corroborates these studies to a certain degree. This correlation varies between linear and non-linear, leaving

questions as to what behavior is in different regions of the graph. The key difference between this data and data previously presented is the velocity range tested. Previous works only covered velocity ranges of 1-32 $\mu\text{m/s}$ [26], and -1 to 5 $\mu\text{m/s}$ [11]. These two ranges cover primarily tip velocities that might be seen in a real-world experimentation on an actual AFM, whereas velocity values selected for this study would be outlandish to test in real world application due to the maximum AFM tip speed being 1-2 microns per second before scanning resolution breaks down [27]. Both studies were done on physical AFMs as well, whereas the discussed results are developed from MD simulation. Regardless of these key differences, the main idea persists that beyond the low-end velocity range presented in previous research, the positive correlation between tip velocity and mean friction persists with small variations throughout.

Also shown in **Figure 7** is the friction coefficient for each specified mean friction. It is important to note that these values are rather low in comparison to real world friction coefficients obtained from physical experimentation [28]. Studies by Penkov et al. found friction coefficients as low as .02 and as high as .6 for graphene samples of varying contact pressures, substrates, and synthesis methods. While the calculated coefficient of friction is around half of what is seen in this study, it must be discussed that this MD simulation format leaves out a lot of environmental factors such as the surrounding air molecules that may contain hydrocarbons which can adhere to the sample, moisture which can change how the AFM tip interacts with the sample, and also the fact that the presented graphene sample is devoid of any atomic scale errors previously touched upon. All these factors not being present lower the friction coefficient of the sample.

Other prior work has delved further into high end velocity regimes like the results from this study. One paper tested a velocity range from 0 to 256 m/s on different configurations of graphene interfaces with the intention of understanding energy dissipation related to graphene friction. The study finds that the friction force increases with increasing velocity, but upon reaching a certain value, decreases with increasing velocity [29]. This threshold value was around 128 m/s, suggesting that further work might be conducted to expand the current data set to fully understand the scope of behavior for graphene velocity in the configuration created for this research. The study then goes on to suggest that friction present in any moving case of graphene may be due to phonon dissipation, or a quantized normal vibration of the crystal lattice structure of a given material. Major differences between this study and the research being covered in this

paper are that the materials and shapes at play are very different. Instead of using an AFM modeled tip made of diamond on a graphene interface, the study uses a graphene sheet sliding over a graphene interface. Another data set obtained via MD simulation tests graphene sheets sliding across a substrate at extremely high speeds to observe what the paper refers to as “ballistic nanofriction” [30]. This data set sees a varying friction leading up to 600 m/s that drops past this threshold. Key differences of the experimental format are that the graphene was dragged across a graphene substrate, and in many cases, a rotational angle was induced on this sheet to observe the effects of misalignment, potentially achieving super lubricity.

Based on the results presented, whether the increasing friction is dependent on contact area fluctuations, it is evident that graphene friction increases with velocity in most part due to increases in atomic interactions between tip atoms and graphene sheet atoms [11]. Thus, as the tip traverses the graphene surface, interaction potentials form and break due to the previously touched upon LJ potential model. As velocity increases, the rate of these interactions goes up, resulting in an increase in friction force.

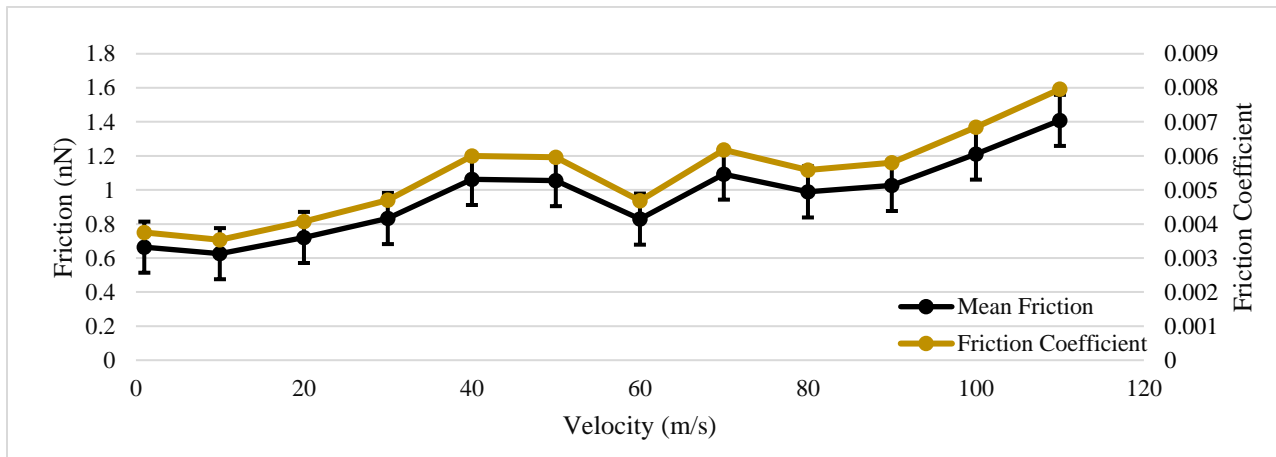


Figure 7 – Friction force and friction coefficient varying at increasing velocity with constant temperature of 300 K and normal load of 177 nN.

3.2 – Temperature Dependent Friction

Another important aspect that influences the frictional properties of 2-D materials and graphene is the amount of thermal energy present in the system. Incidences of atomic interactions and lattice defects may occur spontaneously at varying rates depending on thermal energy. Higher

thermal energy leads to higher incidence rates of these defects, leading to a degree of disorder present at increasing temperatures in crystalline solids [31]. For standard bulk materials with corrugated surface morphologies, this leads to a decrease in friction due to the increased activation of the thermally activated hopping process [32]. For 2D materials like graphene, increase in thermal energy does the exact opposite. As previously discussed, temperature rise in 2D materials leads to an increase in thermally induced dynamic rippling, which causes friction to increase with temperature [32]. Supported 2D materials adhere to their substrate, causing them to behave more like standard bulk materials. To fully understand material behavior in this light, the temperature of the bilayer graphene configuration in this research varied from 300 to 500 Kelvin, with velocity remaining constant.

The previously discussed principles for 2D materials derived from previous studies hold true for data collected in the utilized simulation format. **Figure 8** shows a consistent decrease in friction as temperature increases. Friction coefficient in this respect fluctuates in the same way, decreasing in proportionality with the mean friction value. Previous works have shown similar decreases across the board for relatively low normal load [33]. As previously touched upon in the velocity section, interaction potentials are entirely to blame for decreasing friction here. As temperature is driven up, friction tends to go down under normal testing conditions and normal loads that do not induce structural change in the graphene interface [34]. This decrease is due to the weakening of interatomic potentials which drive friction fluctuations in this context.

The effect discussed for the applied load of 177 nN completely flips when normal load is increased to 885 nN. As expected, the data depicts a higher average friction than that which was present at 188 nN but differs in correlation. Where the lower normal load values saw a decrease in friction with increasing temperature, the high load in **Figure 9** sees a steady increase followed by a jump as the temperature increases to 500 Kelvin. This sharp increase can likely be attributed to the onset of wear due to the increased load combined with high temperature. In prior research, it has been proven that the Young's modulus of graphene varies greatly with temperature [35]. As temperature increases, the Young's modulus decreases, and the shear modulus remains virtually constant. This holds true in the current research, as evidenced by the massive increase in friction spurred by ripping and eventual wear, with graphene physically blocking the movement of the AFM tip because of thermally induced dynamic rippling seen in **Figure 10**.

Further work in temperature dependence seeks to vary the force and temperature over specified ranges to establish a threshold yielding point for each temperature at this configuration, like the established range of Young’s modulus at varying temperature in previous work [22]. This effect, paired with decreases in interatomic potentials and forces between the carbon atoms of the graphene sheet causes the normal load wear point of the graphene specified to decrease as temperature increases. This effect will be delved into further in the following sections as the relationship between contact area and graphene wear is observed.

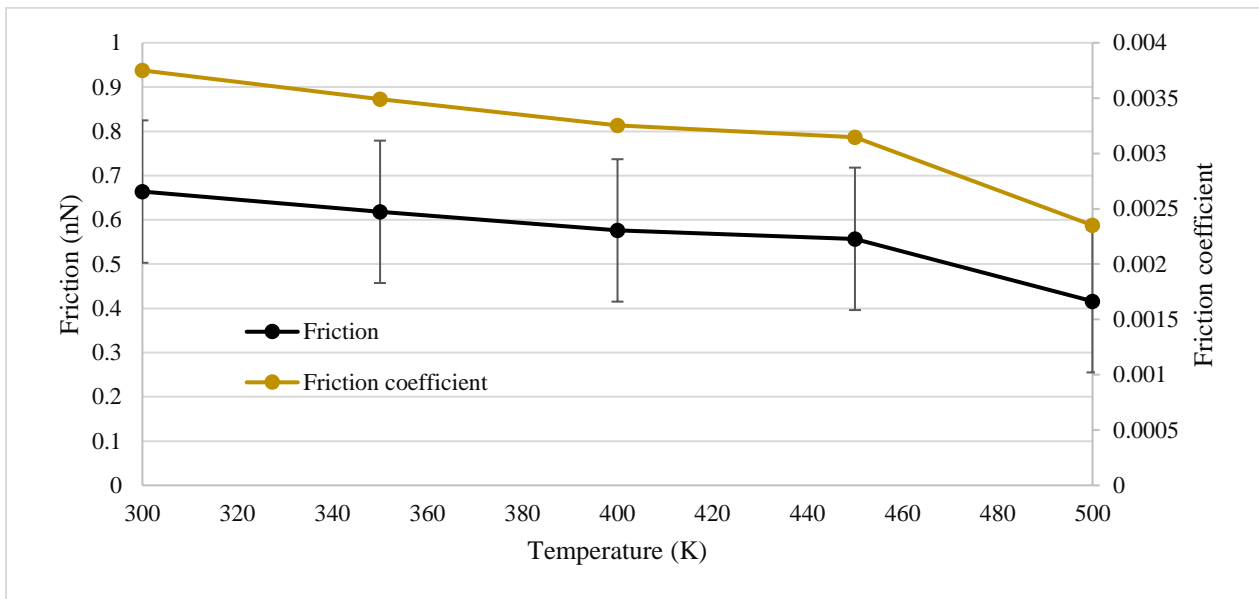


Figure 8 – Friction force and friction coefficient at increasing temperature with constant applied tip velocity of 1 m/s and normal load of 177 nN.

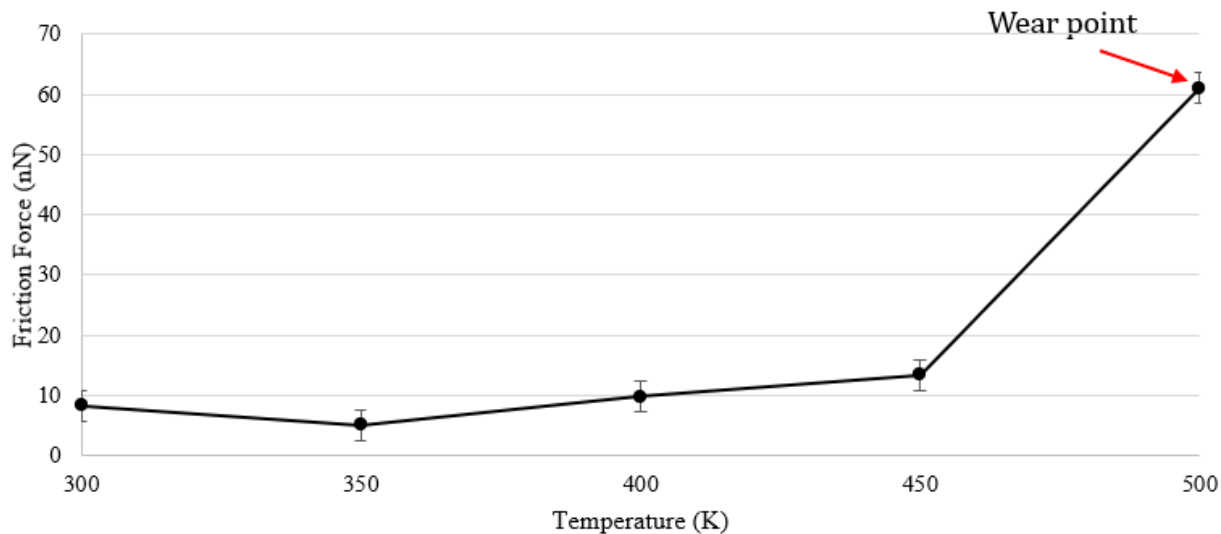


Figure 9 – Friction force at increasing temperature with constant applied tip velocity of 50 m/s for a normal load of 885 nN.

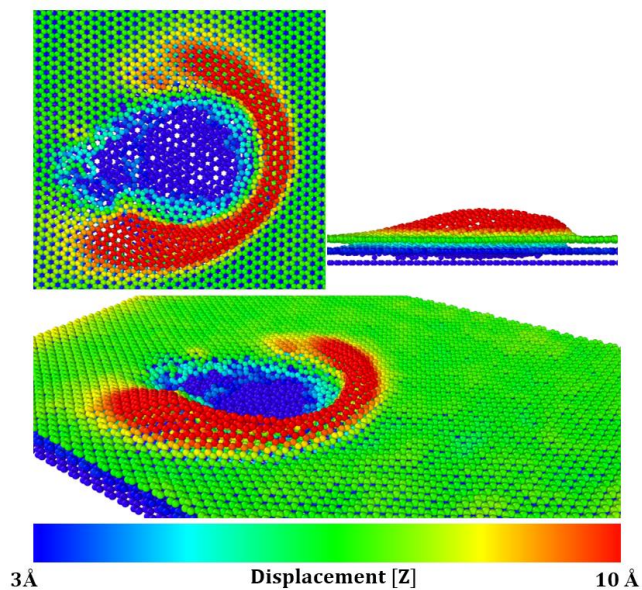


Figure 10 – Ovito visualization of graphene wear seen at 500 K and 885 nN at 50 m/s.

3.3 – Normal Load Dependent Friction

The normal force, or applied load, of bilayer graphene in this study varied from ~10 nN to almost 1000 nN to establish a broad spectrum of behavior for graphene’s friction characteristics at constant temperature and velocity. This covers a fairly low range of load application that has been

studied relatively extensively in previous works and loads that may approach or surpass the yield point for graphene, leading to a shift from friction to wear. Wear behavior will be covered in further work, with friction being the main focal point of this thesis.

In accordance with previous studies, the friction observed at varying normal load on the low end in this research fluctuates somewhat while maintaining a positive trend with increasing load [36]. Previously, it was understood that friction goes up and down at certain normal load values, in the context of this study, that is also the case on the low end as confirmed by **Figure 11**. In the range of ~100 to ~200 nN of load as well as ~400 to ~550 nN of load, the friction first increases, then decreases in the next step, before increasing again at a much higher rate. Surpassing 600 nN, friction maintains constant increase in linear fashion.

Also in **Figure 11** are the comparison values for friction coefficient. Different from the previously discussed values that varied according to changes in temperature and velocity, there are now two variables in the friction equation that are fluctuating: normal force, and friction. Fluctuations in friction were mostly proportional with friction coefficient, however, there were some key differences at low end normal loads in the data set. At high friction force and low normal load, the friction coefficient was significantly larger due to the friction force being large and the normal load being so small, meaning that when the normal load is divided from the friction force, it results in a much higher friction coefficient that is close to values calculated by Penkov et al. which were right around .02 on the low end for a load of ~30 nN [28]. This highlights again how the experiments which obtained much higher friction coefficients differed from the experiments presented in the study. The primary relationship that is revealed from the force relationship shown is that friction coefficient starts out rather large and then decreases substantially with increasing normal load as the number being divided from mean friction gets larger and larger. This continues according to the graph until the normal load reaches around 600 nN when it levels out and continues to fluctuate in proportionality with friction force. The spike at the end, as discussed, is due to wear and the crumpling of graphene sheets as the tip generates wear.

Another occurrence seen in this data run is the wear on the graphene-tip interface. This wear is characterized most evidently by a leap in the friction values occurring as normal load approaches 1000 nN. This behavior occurs due to the graphene beginning to experience load induced dynamic rippling caused by bond breakage and subsequent wear. This rippling effect is not noticeable right before the onset of wear when the applied load is 958 nN seen in **Figure 12a**

and becomes noticeable when the normal load exceeds 1000 nN in **Figure 12b**. The visual of the ripple effect as the normal load surpasses 1000 nN is characterized by a jump in friction from less than 10 nN to almost 35 nN as the graphene begins to pile up onto the AFM tip.

This high normal load application and friction behavior is characteristic of results from a previous study done using an AFM tip that is 10 nm in radius versus the 2 nm one utilized in this work [37]. It is important to note the difference in radius because the referenced study is able to apply far more normal load due to its larger contact radius and therefore larger stress concentrated area. Proportionally speaking, this work and the previously mentioned results experience the same leap once wear and carbon bond breakage begin to occur, validating the current simulation format.

One major factor to point out in the context of this experiment is that these graphene sheets are supported by a substrate. Previous studies dealing with both supported and non-supported graphene have concluded suspended graphene to have a decreasing friction with increasing normal load and supported graphene to have a positive relationship in this aspect. Substrate presence, stiffness, and material can all substantially impact the friction behavior and wear point of a given graphene sample. This is all touched upon in the previous introduction section, but it is important to note as outside data is often synthesized under slightly different conditions.

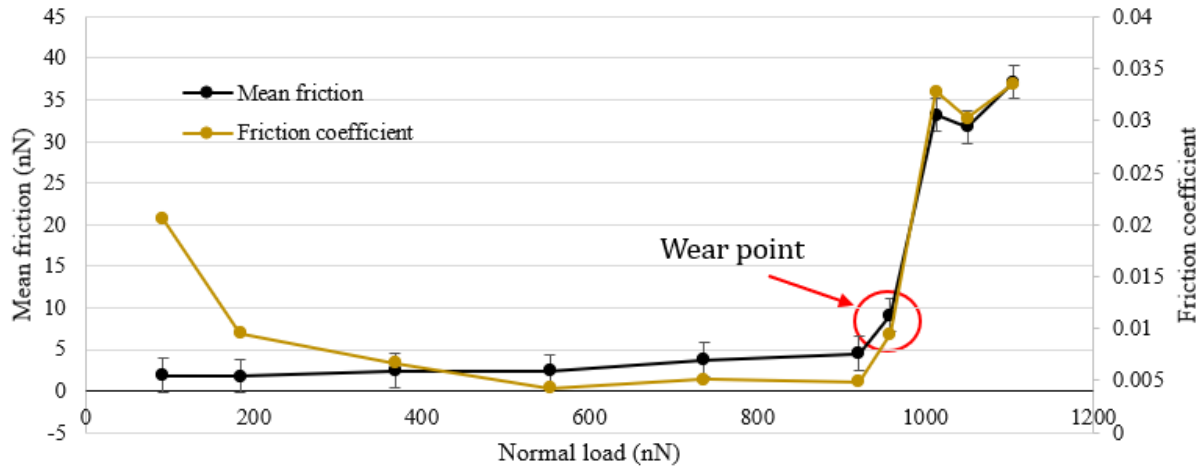


Figure 11 – Normal force dependence of graphene friction force and friction coefficient at constant temperature of 300 K and constant applied tip velocity of 50 m/s.

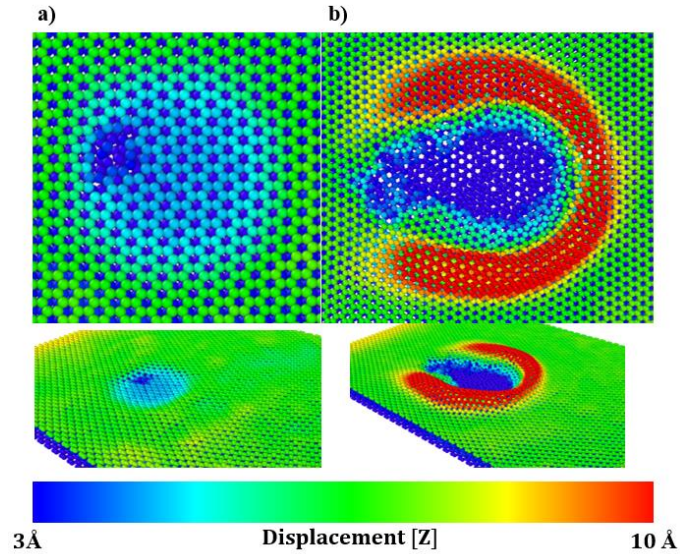


Figure 12 – Ovito renderings for applied loadings of ~ 958 nN (a) and ~ 1013 nN (b).

3.4 – Combined Variable Dependence

As previously touched upon, one of the main goals of the work done thus far was to combine independent variables to conduct factorially designed experimentation and obtain not only a robust data set with results from all three variables, but also individual data sets for each. This is the larger benefit of factorial design as it relates to this study. While it may be time consuming and computationally intensive, creating a larger matrix of values to test is the most effective approach for developing complex relationships between the three independent variables desired.

Prior studies conducted to observe velocity and temperature in combined fashion have drawn the conclusion that the two have a compounding effect when looking at friction, with increasing velocity seeing a decreasing friction at increasing temperatures in every velocity regime [38]. The study being referenced was done using a physical AFM, so velocity ranges remained on the micron per second basis and temperatures did not exceed 150 Celsius, or about 420 Kelvin. In addition, the study focused on two different kinds of graphene samples, one irradiated and one non irradiated. For the sake of this discussion, only the results of the non-irradiated study will be included as radiation application to graphene is outside of the scope of this research. Regardless

of these clear differences, the study is still comparable because of methods and independent variable selection. Results for the non-radiation exposed sample indicated a steady positive relationship between velocity and friction, with each velocity being tested at increasing temperatures. Like results displayed in **Figure 13**, each velocity range was tested at increasing temperature values, resulting in scatter plot showing 3 different data sets. The data shown from the study corroborates the data collected here as they show similar trends with regards to the fact that there is a clear discrepancy between temperatures, and each temperature line increases from left to right on the graph.

One major issue with the data set used is that there is a clear discrepancy present once velocity values of all three temperature ranges pass 60 m/s shown again in **Figure 13**. Leading up to this point, the three increased steadily and showed a somewhat consistent spacing from temperature to temperature. Past this point, the lines become crossed, and it is unclear what kind of correlation exists as there are sharp increases and decreases prior to reaching 90 m/s. The possible solutions to this problem likely fall into the category of re-doing simulations with slightly adjusted parameters such as scanning distance, Gaussian distribution of particle velocities, and maybe even adding more data points for both temperature and velocity in this region to fully grasp exactly what is happening. Unless any of the parameters are changed, or the Gaussian distribution number is fluctuated, two identical input files will produce the exact same result every time they are run. Changing the Gaussian distribution number is a great way to fluctuate results across two simulations with the same temperature, velocity, and normal load, especially if one of those simulations produces numerical data that is outside of expected behavior. For the current set of data, the solution provided is to break down a smaller velocity range of 1 to 50 m/s so a clearer sense of correlation can be discerned. **Figure 14** shows this data visualization, with each bar graph column holding different velocity values and the three different temperature variations. This visual provides a clear correlation within each velocity value and shows that an increase in temperature results in a decrease in mean friction force. As of right now with the prior studies in question, none that have been found include a combination of data at high velocity and temperature variation. As previously discussed, low end velocities in the order of micron per second have been studied with varying temperature, as have high end velocities with no temperature variation, but high-end velocity combined with large temperature variation in the over 300 Kelvin range is somewhat unique to this research.

For the combined study between applied normal load and temperature, results were previously discussed in section 3.3, but an additional graph is provided in **Figure 15** to add further context. For this graph, results from 500 Kelvin were excluded due to the presence of graphene wear outputting a friction value that far exceeded the other data in the set. This graph gives a much clearer picture of the difference in mean friction not only at varying temperatures, but also at varying normal forces. One major issue with the current state of the combined temperature and normal load data is the lack of normal force values tested that lead up to wear. In data from other works, normal load and temperature were varied based on 0 to 300 Kelvin and 0 to 2 GPa [39]. Pressure distribution was significantly more uniform in this study because the model used was a graphene sheet sliding over another graphene sheet, leading to much less potential for wear and most likely the negating of things like rippling and dimpling which lead to huge increases in friction for an AFM formatted experiment such as this one. Comparably, the applied pressure of 0 to 2 GPa only renders around 657 nN of applied force for the contact area utilized in the study, making it a much lower normal load application when considering the contact area for this research is significantly smaller. Results from this work detail that increasing normal load and temperature in this range results in a decreasing friction value. This corroborates data obtained for the 177 nN normal load shown in **Figure 15** but does not corroborate the 885 nN range. This is most likely due again to how close 885 nN is the wear point of the graphene configuration, as depicted by the massive jump in friction at 500 Kelvin in section 3.3.

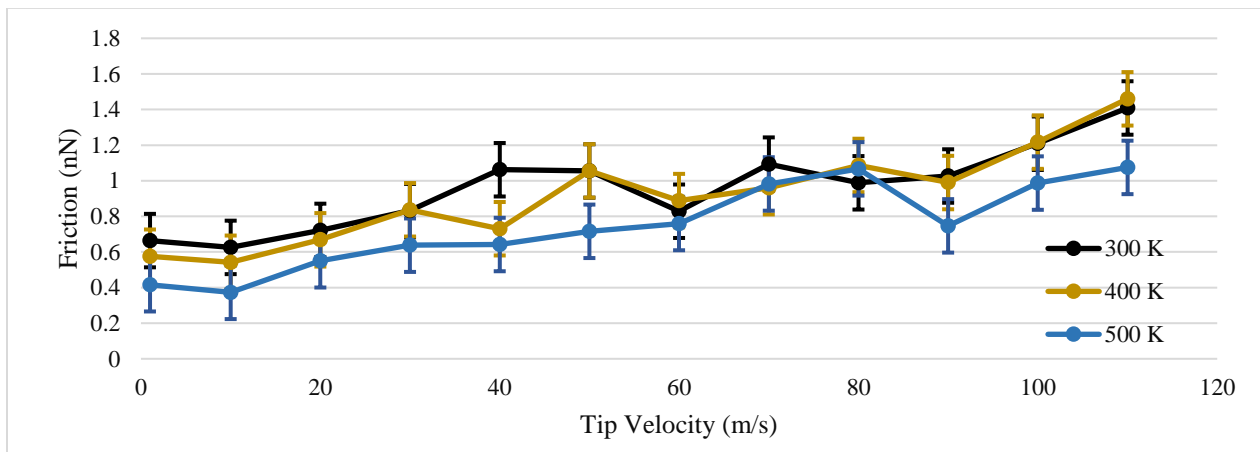


Figure 13 – Friction force measured at varying temperatures and tip velocities with a normal load of 18.42 nN.

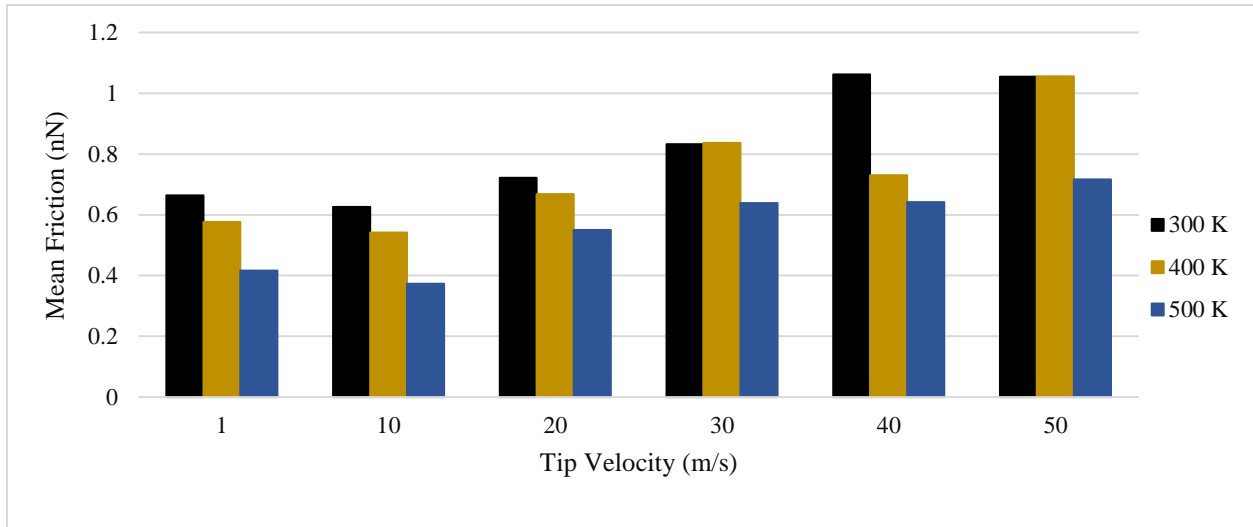


Figure 14 – Friction force at varying tip velocities and temperatures for a velocity range of 1 to 50 m/s, normal load is set to 18.42 nN.

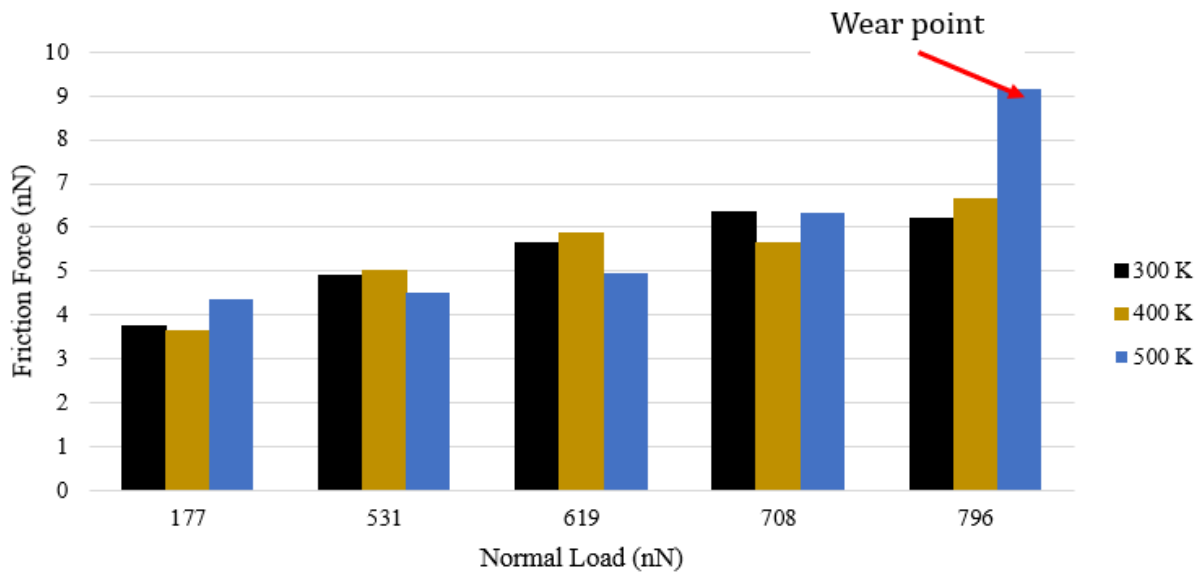


Figure 15 – Friction force at varying temperature and applied normal load with constant applied tip velocity of 50 m/s.

3.5 – Contact Area Dependence

As previously discussed, it has been hypothesized that some kind of relationship exists between contact area and mean friction force exerted by a given sample of graphene. As previously discussed, contact radius is obtained by taking the difference between the two outermost contact atoms between the tip and the sample via the dump file output by LAMMPS as shown in the methods section. This radius value is then used to calculate contact areas at different normal loads, temperatures, and velocities, providing a clear idea of whether fluctuations in friction can be definitively pinned to changes in contact area.

Observing contact area and its relationship with friction, it is important to evaluate past work as a metric of performance for the newly developed data. Contact area is something of utmost importance in tribology due to the impact it has on the overall friction between surfaces. A study conducted by Zhang et al. delves into the frictional behavior of an annular graphene sheet sliding on a graphene substrate [40]. The study tests the friction and contact area behavior at varying normal loads, like this study, and concludes not only that friction increases with increasing contact area, but also that applied load is heavily dependent on this effect [40]. Hence, at the specified low-end applied loads from this work, the friction would increase rather slowly, while at the specified high-end loads used that were almost four times the former, the friction would not only start higher at a lower contact area, but it would jump to rapidly increasing at a given contact area. It is important to note that, different from the data being covered in this work, the experimental configuration in the study being discussed was done not only using different geometry, but also in some cases using a non-rigid substrate, that is the substrate had a stiffness allowing it to move in the z-direction. This is a consideration that may allow for considerable differences when measuring contact area, especially when posed against a rigid substrate.

When evaluating friction varying at both normal load and temperature, another study conducted by Smolyanitsky et al. observed thermally induced dynamic rippling and its impacts on graphene friction [41]. This study was conducted experimentally very similar to the format of this research, with MD simulations being done of monolayer, free-standing graphene sheets under varying load and temperature parameters. The study concluded that fluctuations in friction due to increasing temperature were not attributable to interactions between tip and surface atoms increasing, but rather because of thermally induced dynamic surface roughness behavior. That is,

at increased temperatures, the friction exerted by graphene does not increase or decrease, but instead fluctuates due to dynamic ripples intrinsically present in graphene [41].

Like the previously discussed work by Zhang et al., the data obtained when evaluating both the friction and the contact area at varying applied loads concludes roughly the same idea. Shown in **Figure 16a**, as well as **Figure 16b**, and **Figure 16c**, the friction and contact area curves narrowly match each other in fluctuation. **Figure 16c** does not as closely match in fluctuation between contact area and friction, this may indicate that at this temperature the principle of normal load increasing contact area breaks down, indicating a different mechanism may be causing friction increase such as previously described interatomic energy potentials. One important note for these graphs is the difference in X axis scaling. For all tests done using normal load, data points for friction at wear were excluded to not bog down the data visualization. This is why, for 500 Kelvin, only 3 data points are included because wear occurred once the normal load surpassed ~ 700 nN. **Figure 16d** compares these values previously discussed and shows that varying temperature does not necessarily cause a change in contact area. This concludes that not only is the contact area heavily dependent on normal load, but also that leading up to wear, it is safe to assume that the contact area is going to be proportional to the normal load being applied.

When comparing the normal loads that lead to wear and the corresponding contact areas at increasing temperatures, another important observation can be made. **Figure 15** shows clearly that as the temperature increases, not only does the normal load required to obtain wear decrease, but the associated contact area does the same. This elaborates on the previously made assertion that contact radius and temperature have no relationship at all, and instead suggests that temperature dictates the contact radius at which wear can occur. A lower temperature can increase the contact radius that is required to see graphene wear, while a higher temperature reduces the contact radius needed.

As previously discussed in the work conducted by Smolyanitsky et al., the relationship shown between friction, temperature, and normal load is not straight forward, and is attributed to a variety of variable changes including experimental parameters such as AFM tip size, boundary conditions, and sample size. The results shown in **Figure 17** display the wear points of each temperature and normal load regime tested. In this case, at a wide range of increasing temperatures, the observed normal load that was required to sustain graphene wear decreased as temperature increased. As suggested by Smolyanitsky et al., decrease in normal load wear point at increased

temperatures is most evidently due to the decreasing of inter-atomic bond potentials weakening at increased temperature. This rippling, while not noticed distinctly in this work, can be simplified down to the initial velocity distributions adopted by atoms via the Gaussian velocity distribution in the input file. Because graphene is a 2D material, surface roughness becomes an independent variable instead of remaining static like it does in 3D materials.

Figure 18 delves into another velocity-based study in which contact area and friction fluctuations are compared to one another at changing temperature and velocity. As previously discussed, contact area does not have any discernible correlation with friction or temperature changes. This is shown not only by **Figure 18a** through **Figure 18c**, but also by **Figure 18d**, which extensively drives home the point that contact area does not fluctuate with velocity or temperature change in any significant way. As previously touched upon by Almeida et al., nanoscale friction is dependent on temperature and normal load as well as the mechanical properties of the system [11]. These two properties affect the rate at which atoms on the tip will experience intermolecular interactions with the graphene atoms. Increasing velocity increases the rate of these interactions, causing friction to go up. This corroborates previously discussed temperature dependence of graphene friction in section 3.4 where it was deduced that increases in temperature cause a decrease in friction for a given velocity value prior to wear. The reason for this being that the increase in temperature reduces the strength of intermolecular forces, ultimately reducing their impact and reducing molecular friction.

Another rather interesting study by Liu et al. studies friction behavior of AFM tips on sliding interfaces at varying velocities and manually varied contact areas for both MD simulation and physical experiments. The results found here assert that friction again increases logarithmically with velocity, and when contact radius is directly fluctuated by increasing the AFM tip radius from 1 nm to 2.2 nm along with increasing the tip mass consequentially, there was a resulting increase in friction that paralleled fluctuations seen in physical experiments [42]. This corroborates the points asserted by data collected for this study which concludes that contact area and friction fluctuate in tandem with one another, but, that friction changes do not directly result in a changing contact area. This is shown primarily in **Figure 16** where the mean friction and contact area fluctuate directly with one another as normal load is increased. In **Figure 18**, the contact area is not intentionally changed by applying an increasing normal load, the friction and contact area do not increase in tandem with one another. This study again asserts the idea that

friction generated by changes in velocity is not because velocity changes fluctuate the contact area, but instead because of atomic potential changes as atoms enter and exit energy minima and maxima in each lattice, corroborating findings not only from literature review, but also from data collected regarding the changes in friction versus the changes in contact area at increasing velocity shown in **Figure 18d**, where the contact area does not fluctuate with increasing velocity for any temperature. The friction measured in the work of Liu et al. is governed primarily by equation 5:

$$\frac{1}{\beta k_B T} (F_C - F_L)^{\frac{3}{2}} = \ln\left(\frac{v_0}{v}\right) - \frac{1}{2} \ln\left(1 - \frac{F_L}{F_C}\right) \quad (5)$$

Where F_C and F_L are the mean static friction force at simulation temperature T and 0 Kelvin respectively, and β is a parameter related to lateral friction at low speeds. Additionally, v_0 is a characteristic speed given by a separate equation, v denotes the AFM tip speed, and k_b is Boltzmann's constant. This governing equation dictates not only the inclusion of temperature, normal load, and velocity into the friction calculation for an AFM system, but it also entirely leaves out the contact area, indicating that it may be entirely irrelevant to the friction fluctuations seen here. Liu suggests that were the contact area manually increased using larger normal load or manually increasing the tip radius in the simulation, it would cause friction to compound and generate matching fluctuations. Key differences between the study by Liu et al. and the data collected for this research are primarily related to the materials used in experimentation, with Liu utilizing a gold interface and a silica tip versus the graphene interface and diamond tip utilized in the models of this research. Outside of this, the experimental format for both physical and simulated data is entirely the same, as are the governing principles of interatomic interactions shown.

For yet another work done much earlier by Yoon et al., data collected in physical AFM experiments with intentionally increasing tip radii and normal loads depicts that not only do larger tip radii have a higher friction force at no normal load where purely adhesive forces and tip weight are at play, but they also increase at a higher rate than lower tip radii [43]. This again, corroborates the conclusion of the research in this thesis, which is that independent variables such as velocity and temperature have little to no influence on contact radius between AFM tip and graphene

interface unless paired with increases in normal load or direct changes in tip radii. This principle maintains until the onset of wear and dimple formation when behavior entirely changes.

In short, based on the data presented, the independent variable that plays most into fluctuations in contact area for this study format is normal load. It is determined that contact area does not fluctuate directly with changes in temperature or velocity. Changes in friction at varying temperature and velocity are determined to be attributable to variations in intermolecular forces and mechanical properties of the system. Phenomena such as dynamic rippling, dimple formation, and wear can all have influence on the friction being observed as well. The lasting idea based on data collected by other research as well as the data collected here is that friction and contact area are directly correlated with one another in the context of AFM experimentation and more specifically graphene interfaces by way of the normal load exerted and the size of the sliding surface, not the speed or temperature.

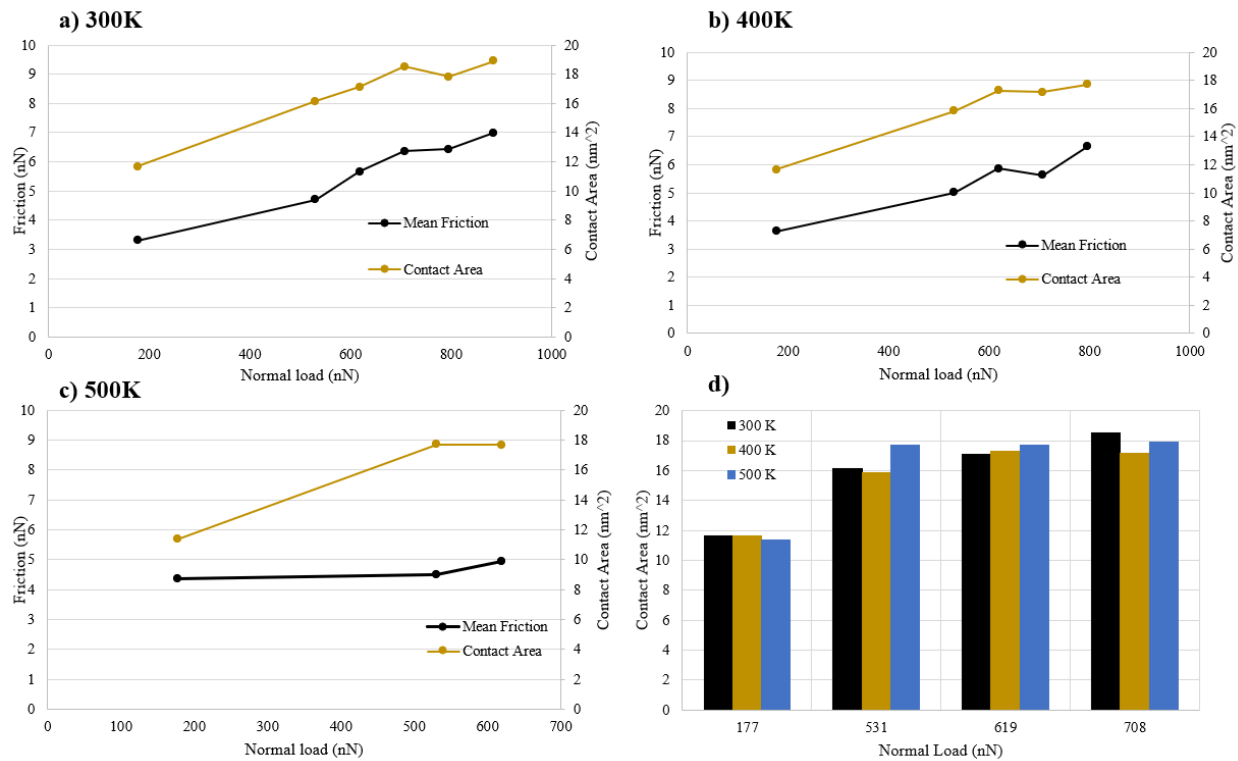


Figure 16 – Mean friction compared to the contact area at a) 300 Kelvin, b) 400 Kelvin, and c) 500 Kelvin, figure 14 d) is a comparison of the contact area across all temperatures and normal loads prior to wear.

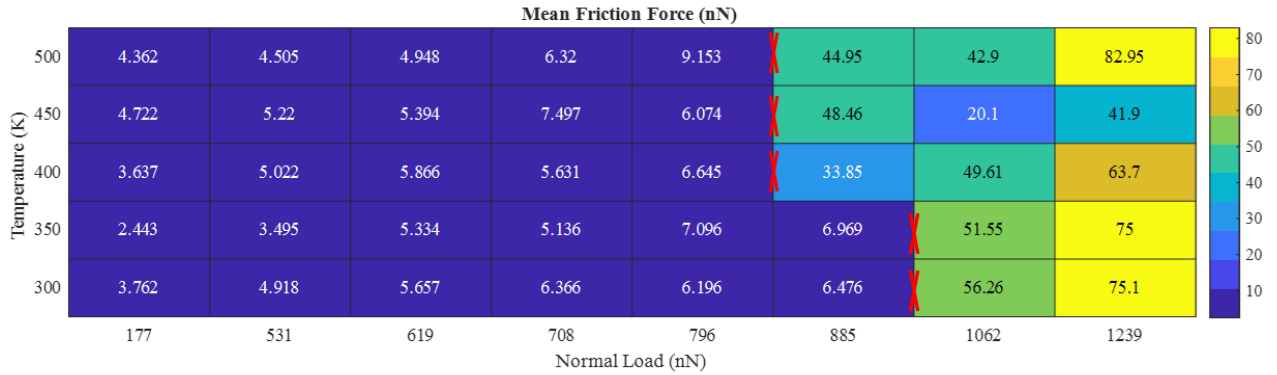


Figure 17 – Wear points at each temperature and normal load with red x marks denoting wear points.

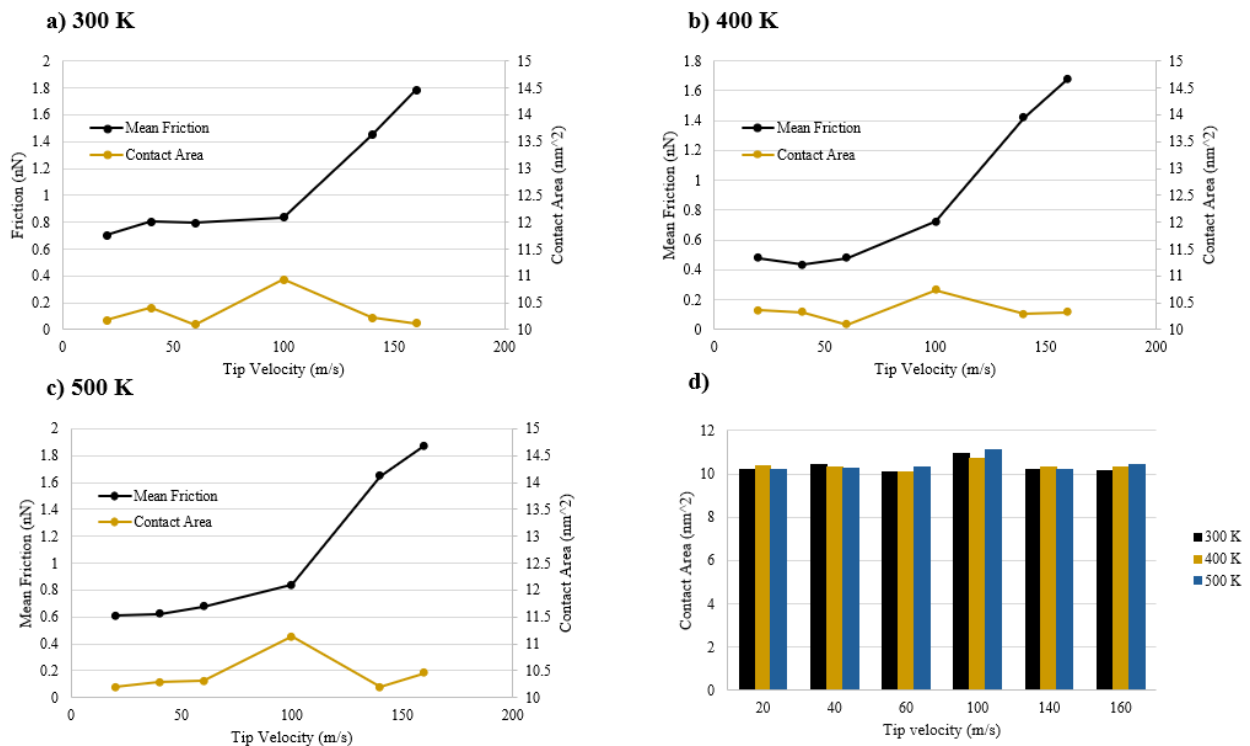


Figure 18 – Mean friction compared to the contact area at a) 300 Kelvin, b) 400 Kelvin, and c) 500 Kelvin, figure 16 d) is a comparison of the contact area across all temperatures and tip velocities, all tests were done at a normal load of 177 nN.

4 – Conclusions

The research discussed above delves into the mechanisms of graphene friction for the independent variables of AFM tip velocity, sample temperature, and normal load. It is initially proposed that graphene friction is caused directly by fluctuations in contact area for all independent variables discussed. Initially, studies are done individually to determine the bilayer graphene friction dependence on velocity, temperature, and normal load. What is concluded is that velocity and normal load have direct discernible positive correlations with graphene friction while temperature has a negative correlation. It is evident that all these occurrences are caused by varying intermolecular interactions, specifically, changing interatomic potentials governed by the kinetic energy, or temperature of the system. The question is posed as to whether the mechanism of these increasing or decreasing instances of interaction can be attributed to changing contact area via any one of the independent variables specified or if they function in tandem with one another. Combined variable study confirms the anticipated results and wear is initialized in the system, with the first noticeable wear point occurring as temperatures reach 500 Kelvin with a ~800 nN normal load. Velocity and temperature combined studies confirm that at every velocity value temperature increases still decrease friction values.

When obtaining measurements for contact area, it becomes clear the mechanisms behind the previously described friction fluctuations can be attributed in some cases to changing contact area, and in others is due to varying interatomic potentials. The verdict on contact area is that it directly impacts friction. That is, changing the area of contact between two bodies, graphene or not, increases the number of inter-atomic interactions occurring, hence increasing the friction. The mechanisms of this increasing this are speculated to be velocity, temperature, or normal load at the advent of this study. It is now clear that fluctuations in contact area can be produced by either increasing the normal load or increasing the size of the surfaces in contact. Changes in friction with velocity and temperature can both hence be attributed to changing interatomic potentials previously discussed. It is important to note that if the contact area were fluctuated by normal load or otherwise, it would thereby increase the number of atoms interacting with each other in the sliding interface of the system, likely increasing friction in all instances of differing velocities and temperatures.

- [1] *Materials Science and Technology*. InTech.
- [2] D. Berman, A. Erdemir, and A. V. Sumant, “Graphene: A new emerging lubricant,” *Materials Today*, vol. 17, no. 1. Elsevier B.V., pp. 31–42, 2014. doi: 10.1016/j.mattod.2013.12.003.
- [3] H. Chen, G. Mi, P. Li, X. Huang, and C. Cao, “Microstructure and tensile properties of graphene-oxide-reinforced high-temperature titanium-alloy-matrix composites,” *Materials*, vol. 13, no. 15, Aug. 2020, doi: 10.3390/ma13153358.
- [4] Z. H. Khan, A. R. Kermany, A. Öchsner, and F. Iacopi, “Mechanical and electromechanical properties of graphene and their potential application in MEMS Mechanical and Electromechanical Properties of Graphene and their Potential Applications in MEMS,” 2017.
- [5] X. Wang, S. Ramírez-Hinestrosa, J. Dobnikar, and D. Frenkel, “The Lennard-Jones potential: when (not) to use it. †”, doi: 10.1039/cXCP00000x.
- [6] H. Li and W. K. Kim, “A comparison study between the Lennard-Jones and DRIP potentials for friction of graphene layers,” *Comput Mater Sci*, vol. 180, Jul. 2020, doi: 10.1016/j.commatsci.2020.109723.
- [7] T. C. O’Connor, J. Andzelm, and M. O. Robbins, “AIREBO-M: A reactive model for hydrocarbons at extreme pressures,” *Journal of Chemical Physics*, vol. 142, no. 2, Jan. 2015, doi: 10.1063/1.4905549.
- [8] M. Höhnerbach and P. Bientinesi, “Optimizing AIREBO: Navigating the Journey from Complex Legacy Code to High Performance,” Oct. 2018, [Online]. Available: <http://arxiv.org/abs/1810.07026>
- [9] G. Rajasekaran, R. Kumar, and A. Parashar, “Tersoff potential with improved accuracy for simulating graphene in molecular dynamics environment,” *Mater Res Express*, vol. 3, no. 3, Mar. 2016, doi: 10.1088/2053-1591/3/3/035011.
- [10] M. Bramowicz, S. Kulesza, and K. Rychlik, “A COMPARISON BETWEEN CONTACT AND TAPPING AFM MODE IN SURFACE MORPHOLOGY STUDIES.”
- [11] F. Ptak, C. M. Almeida, and R. Prioli, “Velocity-dependent friction enhances tribomechanical differences between monolayer and multilayer graphene,” *Sci Rep*, vol. 9, no. 1, Dec. 2019, doi: 10.1038/s41598-019-51103-1.
- [12] Z. Ye, A. Balkanci, A. Martini, and M. Z. Baykara, “Effect of roughness on the layer-dependent friction of few-layer graphene,” *Phys Rev B*, vol. 96, no. 11, Sep. 2017, doi: 10.1103/PhysRevB.96.115401.
- [13] Y. Liao, Z. Li, L. Chen, A. B. Croll, and W. Xia, “Crumpling Defective Graphene Sheets,” *Nano Lett*, vol. 23, no. 8, pp. 3637–3644, Apr. 2023, doi: 10.1021/acs.nanolett.2c04771.
- [14] W. Tian, W. Li, W. Yu, and X. Liu, “A review on lattice defects in graphene: Types generation effects and regulation,” *Micromachines*, vol. 8, no. 5. MDPI AG, 2017. doi: 10.3390/mi8050163.
- [15] Y. Zhang and Y. Shen, “EFFECT OF TEMPERATURE ON NANOSCALE WEAR BEHAVIOR OF GRAPHENE: A MOLECULAR DYNAMICS STUDY,” 2022.

- [16] M. Enachescu, R. J. A. Van Den Oetelaar, R. W. Carpick, D. F. Ogletree, C. F. J. Flipse, and M. Salmeron, "Observation of proportionality between friction and contact area at the nanometer scale," 1999.
- [17] C. N. Shyam Kumar *et al.*, "Nanocrystalline graphene at high temperatures: Insight into nanoscale processes," *Nanoscale Adv*, vol. 1, no. 7, pp. 2485–2494, 2019, doi: 10.1039/c9na00055k.
- [18] L. Y. Lin, D. E. Kim, W. K. Kim, and S. C. Jun, "Friction and wear characteristics of multi-layer graphene films investigated by atomic force microscopy," *Surf Coat Technol*, vol. 205, no. 20, pp. 4864–4869, Jul. 2011, doi: 10.1016/j.surfcoat.2011.04.092.
- [19] "Graphene Characterization." [Online]. Available: www.anton-paar.com
- [20] V. L. Popov, M. Heß, and E. Willert, "Handbook of Contact Mechanics."
- [21] R. Budynas and J. K. Nisbett, *Shigley's Mechanical Engineering Design*, vol. New York. 2015.
- [22] D. Zakarian, A. Khachatrian, and S. Firstov, "Universal temperature dependence of Young's modulus," *Metal Powder Report*, vol. 74, no. 4, pp. 204–206, Jul. 2019, doi: 10.1016/j.mprp.2018.12.079.
- [23] L. M. Collins, J. J. Dziak, and R. Li, "Design of Experiments With Multiple Independent Variables: A Resource Management Perspective on Complete and Reduced Factorial Designs," *Psychol Methods*, vol. 14, no. 3, pp. 202–224, Sep. 2009, doi: 10.1037/a0015826.
- [24] A. Martini, Y. Dong, D. Perez, and A. F. Voter, "Low-speed atomistic simulation of stick-slip friction using parallel replica dynamics," *Tribol Lett*, vol. 36, no. 1, pp. 63–68, Oct. 2009, doi: 10.1007/s11249-009-9460-4.
- [25] R. W. Carpick, A. Martini, and R. J. Cannara, "TITLE: Atomic-Level Stick-Slip BYLINE." [Online]. Available: <http://www.me.upenn.edu/~carpickhttps://engineering.purdue.edu/~martiniahttp://cnst.nist.gov/Staff/cannara.html>
- [26] H. Lang, Y. Peng, K. Zou, Y. Huang, and C. Song, "Velocity-Dependent Friction of Graphene at Electrical Contact Interfaces," *Langmuir*, vol. 39, no. 32, pp. 11363–11370, Aug. 2023, doi: 10.1021/acs.langmuir.3c01197.
- [27] H. -J BUTT *et al.*, "Scan speed limit in atomic force microscopy," *J Microsc*, vol. 169, no. 1, pp. 75–84, 1993, doi: 10.1111/j.1365-2818.1993.tb03280.x.
- [28] O. Penkov, H. J. Kim, H. J. Kim, and D. E. Kim, "Tribology of graphene: A review," *International Journal of Precision Engineering and Manufacturing*, vol. 15, no. 3. SpringerOpen, pp. 577–585, 2014. doi: 10.1007/s12541-014-0373-2.
- [29] Y. Dong *et al.*, "Velocity-dependent phononic friction in commensurate and incommensurate states," *Tribol Int*, vol. 180, Feb. 2023, doi: 10.1016/j.triboint.2023.108224.
- [30] Y. Liu, F. Grey, and Q. Zheng, "The high-speed sliding friction of graphene and novel routes to persistent superlubricity," *Sci Rep*, vol. 4, May 2014, doi: 10.1038/srep04875.
- [31] A. Alivaliollahi, G. Alahyarizadeh, and A. Minucmehr, "Effect of temperature, pressure, crystal defect types, and densities on the mechanical behavior of tungsten under tensile deformation: A molecular dynamics simulation study," *Nuclear Materials and Energy*, vol. 37, Dec. 2023, doi: 10.1016/j.nme.2023.101555.

- [32] D. Berman, A. Erdemir, and A. V. Sumant, "Approaches for Achieving Superlubricity in Two-Dimensional Materials," *ACS Nano*, vol. 12, no. 3. American Chemical Society, pp. 2122–2137, Mar. 27, 2018. doi: 10.1021/acsnano.7b09046.
- [33] J. Li, Y. Peng, X. Tang, Z. Yang, C. Chen, and L. Bai, "Load-oriented thickness-dependent friction behavior of graphene supported by substrate with different stiffnesses," *Comput Mater Sci*, vol. 203, Feb. 2022, doi: 10.1016/j.commatsci.2021.111164.
- [34] P. Kumar and M. F. Wani, "Effect of temperature on the friction and wear properties of graphene nano-platelets as lubricant additive on Al-25Si alloy," *Mater Res Express*, vol. 6, no. 4, 2019, doi: 10.1088/2053-1591/aafb46.
- [35] L. Shen, H. S. Shen, and C. L. Zhang, "Temperature-dependent elastic properties of single layer graphene sheets," *Mater Des*, vol. 31, no. 9, pp. 4445–4449, Oct. 2010, doi: 10.1016/j.matdes.2010.04.016.
- [36] Z. Ye and A. Martini, "Atomistic simulation of the load dependence of nanoscale friction on suspended and supported graphene," *Langmuir*, vol. 30, no. 49, pp. 14707–14711, Dec. 2014, doi: 10.1021/la503329u.
- [37] Q. Xu, X. Li, J. Zhang, Y. Hu, H. Wang, and T. Ma, "Suppressing Nanoscale Wear by Graphene/Graphene Interfacial Contact Architecture: A Molecular Dynamics Study," *ACS Appl Mater Interfaces*, vol. 9, no. 46, pp. 40959–40968, Nov. 2017, doi: 10.1021/acscami.7b11133.
- [38] Y. Gongyang *et al.*, "Temperature and velocity dependent friction of a microscale graphite-DLC heterostructure," *Friction*, vol. 8, no. 2, pp. 462–470, Apr. 2020, doi: 10.1007/s40544-019-0288-0.
- [39] X. Gao, W. Ouyang, M. Urbakh, and O. Hod, "Superlubric polycrystalline graphene interfaces," *Nat Commun*, vol. 12, no. 1, Dec. 2021, doi: 10.1038/s41467-021-25750-w.
- [40] H. Zhang, J. Qu, Z. Guo, L. Huang, and Q. Xie, "Negative area-dependent nanoscale friction of annular graphene sheets," *AIP Adv*, vol. 12, no. 11, Nov. 2022, doi: 10.1063/5.0117212.
- [41] A. Smolyanitsky, "Effects of thermal rippling on the frictional properties of free-standing graphene."
- [42] X. Z. Liu, Z. Ye, Y. Dong, P. Egberts, R. W. Carpick, and A. Martini, "Dynamics of Atomic Stick-Slip Friction Examined with Atomic Force Microscopy and Atomistic Simulations at Overlapping Speeds," *Phys Rev Lett*, vol. 114, no. 14, Apr. 2015, doi: 10.1103/PhysRevLett.114.146102.
- [43] E. S. Yoon, R. A. Singh, H. J. Oh, and H. Kong, "The effect of contact area on nano/micro-scale friction," *Wear*, vol. 259, no. 7–12, pp. 1424–1431, Aug. 2005, doi: 10.1016/j.wear.2005.01.033.